Zeolite Engineering

Deutsche Ausgabe: DOI: 10.1002/ange.201608417
Internationale Ausgabe: DOI: 10.1002/anie.201608417

The Mosaic Structure of Zeolite Crystals

*Zhengxing Qin, Georgian Melinte, Jean-Pierre Gilson, Maguy Jaber, Krassimir Bozhilov, Philippe Boullay, Svetlana Mintova, Ovidiu Ersen, and Valentin Valtchev**

Abstract: *Zeolites are widely used in many commercial processes, mostly as catalysts or adsorbents. Understanding their intimate structure at the nanoscale is the key to control their properties and design the best materials for their ever increasing uses. Herein, we report a new and controllable fluoride treatment for the non-discriminate extraction of zeolite framework cations. This sheds new light on the sub-structure of commercially relevant zeolite crystals: they are segmented along defect zones exposing numerous nanometer-sized crystalline domains, separated by low-angle boundaries, in what were apparent single-crystals. The concentration, morphology, and distribution of such domains analyzed by electron tomography indicate that this is a common phenomenon in zeolites, independent of their structure and chemical composition. This is a milestone to better understand their growth mechanism and rationally design superior catalysts and adsorbents.*

Zeolites are widely used in petroleum refining and petrochemical processes.[1–3] In the future, their impact will widen to process heavier fossil and renewable feedstocks.[4,5] A feature making zeolites such unique materials is their remarkable shape-selectivity, giving them formidable advantages over other catalysts.[6] However, this comes at the cost of limited accessibility to and restricted diffusion in their sub-nanometer-sized microporosity.[7,8] While the general field of mass transport in zeolites is very lively,[9] the precise impact of their crystal substructures on mass transport is scarcely mentioned. A comprehensive investigation of zeolite substructures showed that large (micron-sized) zeolite crystals display intergrown structures consisting of up to 11 subunits; the resulting interfaces between the subunits generate diffusion barriers.[10] However, the impact of these extended defective structures is relatively limited because molecules rarely penetrate deeply inside such large crystals. Local defective structures on the other hand, such as planar defects and grain boundaries, are expected to have more significant effects on transport phenomena and catalytic performances. Thus far, their characterization and quantification was difficult and visualizing their effect on the volume of an entire crystal nearly impossible.

Our previous work showed that a HF-NH_4F solution readily removes both framework Si and Al, dissolves preferentially lattice defects and forms mesopores.[11] However, HF raises some safety issues and the fast kinetics renders the process difficult to control. Recently, we discovered that zeolite etching in pure NH_4F solutions is equally efficient and more controllable.[12] NH_4F undergoes double hydrolysis reactions in aqueous solutions and a limited and controlled amount of HF is in equilibrium with F^- (**1** and **2** in Figure 1).

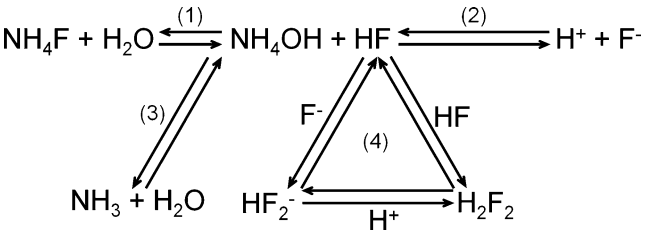

Figure 1. Species present in a NH_4F aqueous solution. 1) Double hydrolysis of ammonium fluoride. 2) Dissociation of HF. 3) Double hydrolysis of NH_4OH. 4) Equilibria between HF and bifluoride species.

Some other fluoride species, for example, HF_2^-, are also present (**4** in Figure 1); they dissolve Si and Al at equal rates and the zeolite framework etching starts immediately in such NH_4F solutions (prompt release of NH_3 and increase of solution pH (**3**, Figure 1).[11] Such etching is therefore moderate due to the low concentration of active fluoride species, produced in situ when needed. Consumption of these active fluorides shifts the double hydrolysis equilibrium of NH_4F and ensures that the removal of framework cations proceeds under mild and controllable conditions. Zones more vulnerable to chemical attack, such as interfaces between intergrown crystals and grain boundaries, are first dissolved, revealing the intimate substructures of zeolite crystals.[11] We illustrate this method on a series of commercially available and home-made MFI type zeolites (Supporting Information, Table S1).

[*] Dr. Z. Qin, Prof. J.-P. Gilson, Dr. S. Mintova, Dr. V. Valtchev
Laboratoire Catalyse et Spectrochimie
Normandie Univ, ENSICAEN, UNICAEN, CNRS
6 Bd Maréchal Juin, 14000 Caen (France)
E-mail: valentin.valtchev@ensicaen.fr
Dr. G. Melinte, Prof. O. Ersen
Institut de Physique et de Chimie de Strasbourg
Université de Strasbourg
23, rue du L oess BP 43, 67034 Strasbourg (France)
Prof. M. Jaber
Laboratoire d'Archéologie Moléculaire et Structurale
Sorbonne Universités, UPMC Univ Paris 06, CNRS
4 place Jussieu, 75005 Paris (France)
Prof. K. Bozhilov
Central Facility for Advanced Microscopy and Microanalysis
University of California
Riverside 900 University Avenue, Riverside, CA 92521 (USA)
Dr. P. Boullay
CRISMAT, Normandie Univ, ENSICAEN, UNICAEN, CNRS
6 Bd Maréchal Juin, 14000 Caen (France)
Supporting information and the ORCID identification number(s) for the author(s) of this article can be found under http://dx.doi.org/10.1002/anie.201608417.

The fluoride treatment of complex intergrown aggregates, illustrated by ZSM-5-I, clearly highlights the preferential dissolution of the interface between crystals (Figures 2a–d and S1). After a 5 minute etching, individual crystals in an aggregate clearly appear. The periphery contains well-formed parallel crystals (ZSM-5-I-5; Figure 2b and Figure S1b) while its core is made of much smaller anhedral crystallites (Figure 2b). After 20 min, further segmentation and surface dissolution of zeolite particles occurs (Figures 2c and S1c). Analysis of the crystalline debris reveals zones of preferential dissolution in apparent single-crystals (Figures 2c and S1e). Further dissolution results in sponge-like structures with about 50% of mesopore volume (Figures 2d and S1d, Table S1). Rectangular *meso*-pores are observed in each single particle (Figure 2d). Although highly segmented and deeply etched, the zeolite retains a high crystallinity and a micropore volume characteristic of a highly crystalline MFI (Table S1 and Figure S2).

Apparent single-crystals (ZSM-5-II; Figure S3a,c) are also etched using the same procedure. During the early stage of dissolution, twin crystals separate and pseudo monocrystals are segmented along hitherto hidden defect zones (ZSM-5-II-15; Figure S3b,d). A closer inspection reveals a mosaic of 10 to 20 nm rectangular voids (Figure 2e) with straight and well-defined edges, in good agreement with N_2 physisorption results (Figure S4a, b). Although not perfectly aligned, most have similar orientations. Upon further etching (30 min), the mosaic of rectangular mesopores further develops (Figures 2f and S4b). After 60 min, many cages interconnect to form larger pores. The structure of the resulting sample, ZSM-5-II-60, is very open and displays 30–40 nm rectangular mesopores (Figures 2g, S3e, S4b) with thin (10–30 nm) walls while crystallinity (Figures 2h and S4c) and micropore volume (Table S1) are retained.

To provide deeper insights in the dissolution process, we resorted to electron tomography, a powerful method to characterize in 3D hierarchical materials.[13] Most of the pores in the 15 min treated sample are isolated (Figures 3 and S5). They exhibit rectangular shape (Figures 3a,c,d and S5c), and a 3D reconstruction (Figure S5c) shows a roughly cubic shape. Occasionally, neighboring pores connect by the dissolution of a relatively thin dividing wall (Figure S5b). The relatively uniform distribution of mesopores appears clearly in a reconstruction (15 min treated crystal; Movie S1). The number of pores and their surface per unit zeolite volume can also be evaluated by tomography. Using only the most

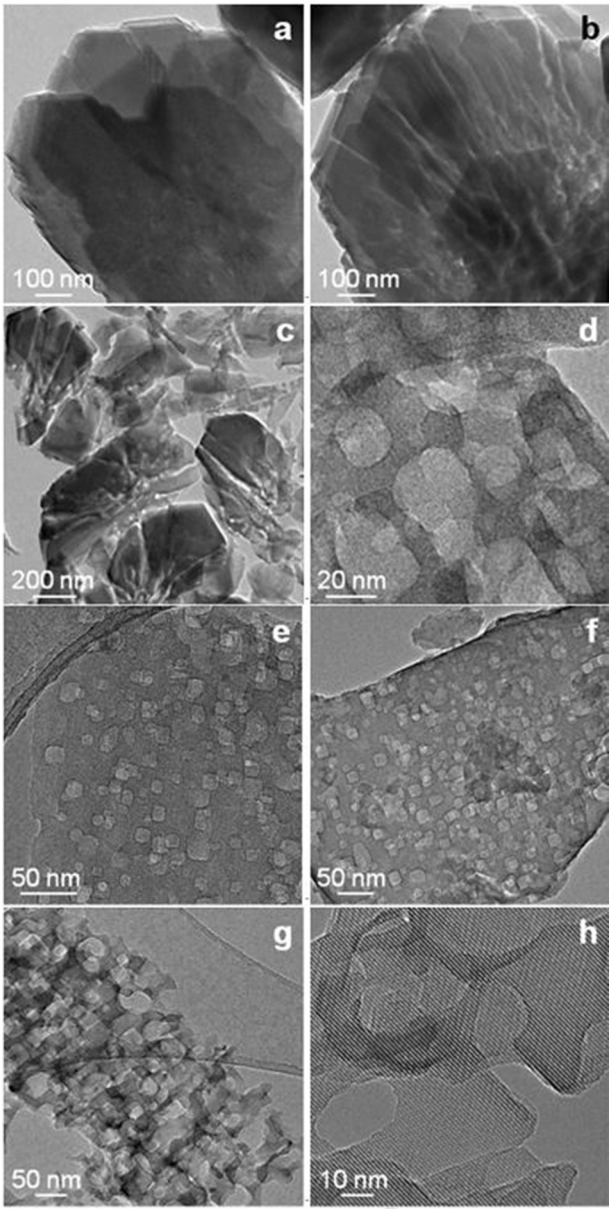

Figure 2. TEM monitoring of the dissolution of aggregates (ZSM-5-I) and apparent single-crystals (ZSM-5-II). a) Parent ZSM-5-I, b) ZSM-5-I-5, c) ZSM-5-I-20, and d) ZSM-5-I-60 obtained after 5, 20, and 60 min of fluoride treatment, respectively. e) ZSM-5-II-15, f) ZSM-5-II-30, and g,h) ZSM-5-II-60 obtained after fluoride treatment of ZSM-5-II for 15, 30, and 60 min, respectively.

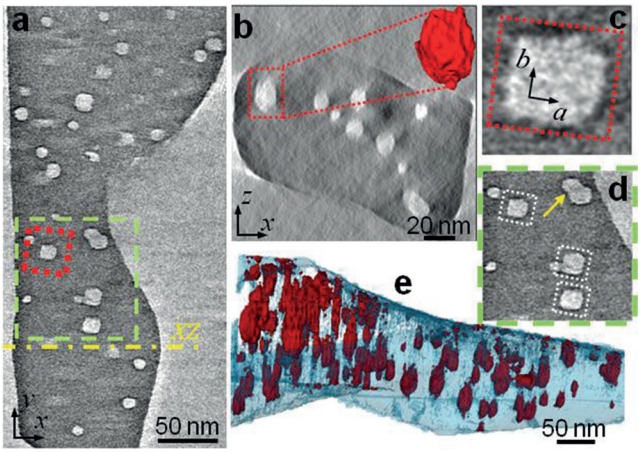

Figure 3. a) XY slice clipped through the center of the 3D model of 15 min treated ZSM-5-II (Movie S1). The yellow line in (a) shows the position of the XZ slice presented in (b). The red inset in (b) shows the 3D morphology of the pore highlighted in rectangle. c,d) cropped regions of the XY slice highlight the rectangle pores. d) Isolated mesopores with similar orientation (white rectangles) and pore with less-defined morphology (yellow arrow) owing to the merger of neighboring pores. e) Snapshots of the 3D model acquired at XY–b direction (zeolite body in transparent blue, pores in red).

accurate data, the density of dissolved domains in the 15 min treated sample ranges from 35 to 90 per 10^6 nm^3. Taking an average of 70 pores per 10^6 nm^3, the overall area of the grain boundaries is 90000 nm^2. The mesopore volume of different particles, computed from electron tomography, ranges between 155 and 470 Å^3, that is, a mesoporosity of 3 to 9%, assuming a unit cell volume of 5211.28 Å^3.[14] After a 30 min etching, up to 90% of the mesopores are interconnected and linked to the external surface (Figure S6). The expansion of the mesoporous network (60 min) leads to a sponge-like structure (Figure S7).

A mosaic pattern of rectangular and aligned pores is observed in both commercial samples. This is also observed in a homemade ZSM-5 (ZSM-5-III; Figure S8), a silicalite-1 (Figure S9), the all-silica analogue of ZSM-5, and in a MOR-type zeolite (Figure S10), indicating that such defect zones are probably quite widespread among zeolite types. Indeed, the interfaces between intergrown MOR crystals also dissolve first and then the individual crystals are etched to form rectangular pores with a size and a density similar to those observed in ZSM-5 crystals. In recent, yet unreported, scouting experiments, we observed similar dissolution patterns with other important zeolites (FER, FAU). In other words, all of the zeolites processed so far display an astonishing high number of aligned nano-pores after a NH_4F treatment, indicating that this phenomenon is ubiquitous, that is, not limited to specific structure types nor restricted to narrow chemical composition ranges. It is difficult to rationalize such a phenomena solely by the random dissolution of Si and Al, as this would result in pores with ill-defined shapes.[15,16] We reported elsewhere that the dissolution, in HF-NH_4F mixed solutions, of aggregated and twin zeolite crystals always starts preferentially at the interfaces between defined subunits.[11,17] Our present results show that a similar dissolution phenomenon takes also place in a pure NH_4F solution. The timely release of active fluoride species in the latter case allows a much better control of the dissolution of zeolites, leading to a chemical etching with a precision of a few nm^3. Considering the uniformity of shape, boundary regularity and consistent orientation of the pores, we attribute their formation to the removal of small grains with well-defined boundaries. This unambiguously indicates that zeolite crystals are inherently made of numerous nano-domains with well-defined sizes, shapes, and structures. Such regular nanocrystalline domains are not limited to the handful of macroscopically observable intergrowths.[10,18,19]

These nano-sized domains are most probably a direct consequence of the nucleation mechanism in zeolite synthesis (Figure 4). The most accepted mechanism of formation of many zeolites, including the MFI-type, is oriented aggregation.[20–23] Rimer and co-workers showed recently that anchoring precursor particles to growing zeolite faces is a commonly observed phenomenon.[22,23] It follows that the arrangement of zeolite domains is decisive for the subsequent growth of a zeolite crystal.[21,23] Such imperfect particles, rotated or tilted with respect to growing terraces, can easily lead to the formation of a crystalline domain with a distinct interface.[24,25] Thus, crystal dissolution with NH_4F, reveals the inherent mosaic structure of zeolites, and provides a new and

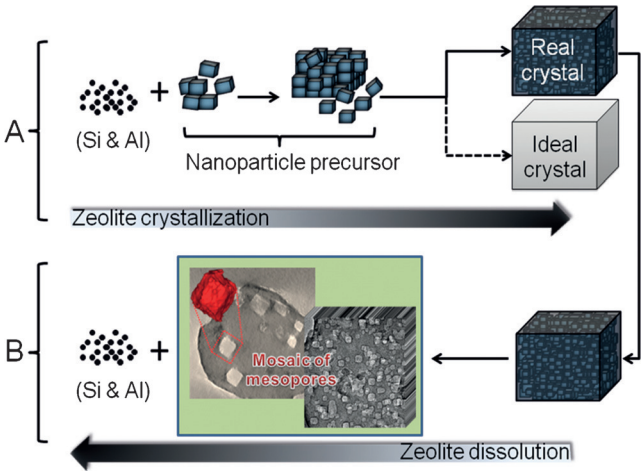

Figure 4. Zeolite growth process (A) and its dissolution in fluoride medium (B) revealing the mosaic structure of zeolite crystals. Green inset: right, TEM of 30 min treated ZSM-5-II; left, magnified view of 15 min treated ZSM-5-II with 3D model of a generated mesopore (red).

deeper understanding of the nano-scale architecture during zeolite crystallization (Figure 4).

Additionally, NH_4F etching is a new tool to improve the mass transport and thus the catalytic properties of zeolites. Here, *meta*-xylene (*m*-X, kinetic diameter of 0.68 nm) isomerization and 1,3,5-triisopropylbenzene (TiPBz, kinetic diameter of 0.95 nm) dealkylation are selected to highlight the catalytic effects of fluoride etching, on the whole zeolite (*m*-X) and specifically on its external surface (TiPBz). Figure 5a shows that the *m*-X conversion on treated ZSM-5-II systematically increases with treatment severity. Because all of the Si/Al are nearly identical, this increase is due to the removal of diffusion barriers and a shortening of the diffusion path length of reactants and products.[26] Figure 5b indicates that removing local defects of the zeolite dramatically increases the catalytic performance of its external surface; this is the result of better accessibility, lowering of surface barriers coupled with excellent intrinsic activity.

An obvious potential application of the fluoride etching is the direct preparation of advanced materials, such as nanosheets[27] or monocrystalline "house of cards"[28] (Figure 2g), heretofore prepared solely by bottom–up approaches. An area of future research would be finer control of these "defects" during the large-scale synthesis of commercial zeolites making materials more amenable to tailored post-synthesis modifications. One of the most important general outcomes of this discovery is that all commercially available micron-sized zeolite crystals have the potential to be transformed in nano-sized crystals, with all of the benefits these can bring (such as removal of important barriers to diffusion and catalysis) without their current disadvantages (difficult separation of the nanocrystals from their mother liquor, dedicated synthesis protocols); this would contribute greatly to meet the growing and exacting requirements of modern microporous-based catalysts and adsorbents.

In summary, this new fluoride etching method, easy to implement and control, readily extracts both framework

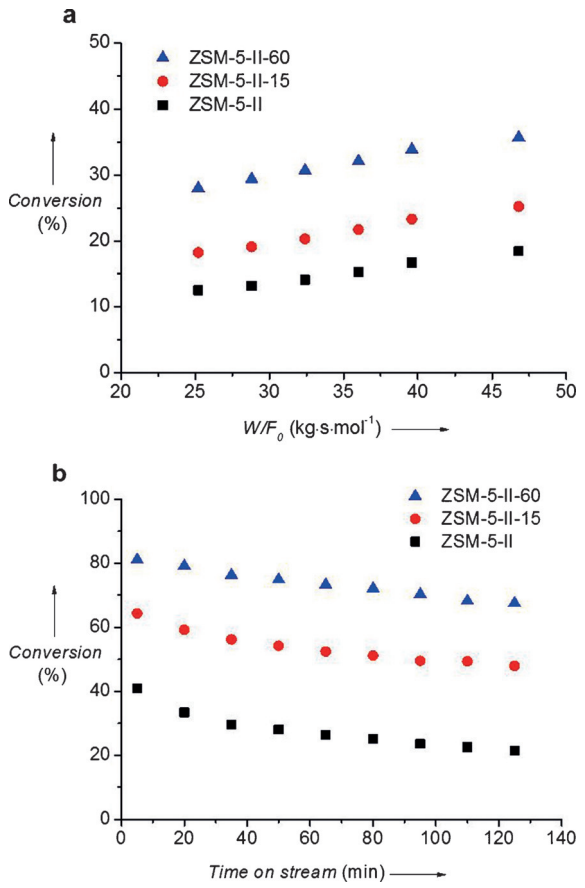

Figure 5. Conversion of a) *m*-X ($T = 623$ K, $P = 0.101$ MPa, W/F_0: 25–47 kg s mol^{-1}); b) TiPBz ($T = 623$ K, $P = 0.101$ MPa, $W/F_0 = 380$ kg s mol^{-1}) on the parent ZSM-5-II and its NH_4F-treated derivatives, after 15 and 60 min treatments.

cations (Si and Al) and preferentially dissolves lattice defects. As it progresses, it removes small but numerous defect zones in zeolite crystals revealing high concentrations of nanocrystalline domains with defined grain boundaries. A deeper analysis of these crystal imperfections will contribute greatly to better understand the fundamental rules of crystal growth in zeolites. Additionally, the contribution of these physical barriers needs to be taken into account to better analyze and understand mass transport phenomena in zeolites.

Acknowledgements

This study was sponsored by ANR-15-CE06-0004-02 (DirectCatSynBioFuel).

Keywords: crystal engineering · fluoride etching · nanostructures · zeolites

How to cite: *Angew. Chem. Int. Ed.* **2016**, *55*, 15049–15052
Angew. Chem. **2016**, *128*, 15273–15276

[1] A. Corma, *Chem. Rev.* **1995**, *95*, 559–614.
[2] W. Vermeiren, J. P. Gilson, *Top. Catal.* **2009**, *52*, 1131–1161.
[3] C. Martínez, A. Corma, *Coord. Chem. Rev.* **2011**, *255*, 1558–1580.
[4] T. F. Degnan, *Curr. Opin. Chem. Eng.* **2015**, *9*, 75–82.
[5] T. Ennaert, J. V. Aelst, J. Dijkmans, R. D. Clercq, W. Schutyser, M. Dusselier, D. Verboekend, B. F. Sels, *Chem. Soc. Rev.* **2016**, *45*, 584–611.
[6] D. W. Breck, *Zeolite Molecular Sieves: Structure, Chemistry, and Use*, Wiley, New York, **1974**.
[7] V. Valtchev, L. Tosheva, *Chem. Rev.* **2013**, *113*, 6734–6760.
[8] K. Möller, T. Bein, *Chem. Soc. Rev.* **2013**, *42*, 3689–3707.
[9] J. Kärger, D. M. Ruthven, D. N. Theodorou, *Diffusion in Nanoporous Materials*, Wiley-VCH, Weinheim, **2012**.
[10] L. Karwacki, M. H. F. Kox, D. A. M. de Winter, M. R. Drury, J. D. Meeldijk, E. Stavitski, W. Schmidt, M. Mertens, P. Cubillas, N. John, A. Chan, N. Kahn, S. R. Bare, M. Anderson, J. Kornatowski, B. M. Weckhuysen, *Nat. Mater.* **2009**, *8*, 959–965.
[11] Z. Qin, L. Lakiss, J. P. Gilson, K. Thomas, J. M. Goupil, C. Fernandez, V. Valtchev, *Chem. Mater.* **2013**, *25*, 2759–2766.
[12] V. Valtchev, J. P. Gilson, Z. Qin (CNRS), WO 2016005783 A1, **2016**.
[13] Y. Wei, T. E. Parmentier, K. P. de Jong, J. Zečević, *Chem. Soc. Rev.* **2015**, *44*, 7234–7261.
[14] (http://izasc.biw.kuleuven.be/fmi/xsl/IZA-SC/ftc_fw.xsl?-db = Atlas_main&-lay = fw&-max = 25&STC = MFI&-find), accessed on 27 March **2016**.
[15] J. C. Groen, T. Bach, U. Ziese, A. M. Paulaime-van Donk, K. P. de Jong, J. A. Moulijn, J. Pérez-Ramírez, *J. Am. Chem. Soc.* **2005**, *127*, 10792–10793.
[16] K. P. de Jong, J. Zečević, H. Friedrich, P. E. de Jongh, M. Bulut, S. van Donk, R. Kenmogne, A. Finiels, V. Hulea, F. Fajula, *Angew. Chem. Int. Ed.* **2010**, *49*, 10074–10078; *Angew. Chem.* **2010**, *122*, 10272–10276.
[17] Z. Qin, J. P. Gilson, V. Valtchev, *Curr. Opin. Chem. Eng.* **2015**, *8*, 1–6.
[18] E. Stavitski, M. R. Drury, D. A. M. de Winter, M. H. F. Kox, B. M. Weckhuysen, *Angew. Chem. Int. Ed.* **2008**, *47*, 5637–5640; *Angew. Chem.* **2008**, *120*, 5719–5722.
[19] Z. Ristanović, J. P. Hofmann, U. Deka, T. U. Schülli, M. Rohnke, A. M. Beale, B. M. Weckhuysen, *Angew. Chem. Int. Ed.* **2013**, *52*, 13382–13386; *Angew. Chem.* **2013**, *125*, 13624–13628.
[20] J. F. Banfield, S. A. Welch, H. Zhang, T. T. Ebert, R. L. Penn, *Science* **2000**, *289*, 751–754.
[21] T. M. Davis, T. O. Drews, H. Ramanan, C. He, J. Dong, H. Schnablegger, M. A. Katsoulakis, E. Kokkoli, A. V. McCormick, R. L. Penn, M. Tsapatsis, *Nat. Mater.* **2006**, *5*, 400–408.
[22] A. I. Lupulescu, J. D. Rimer, *Science* **2014**, *344*, 729–732.
[23] M. Kumar, H. Luo, Y. Roman-Leshkov, J. D. Rimer, *J. Am. Chem. Soc.* **2015**, *137*, 13007–13017.
[24] J. J. De Yoreo, P. U. P. A. Gilbert, N. A. J. M. Sommerdijk, R. L. Penn, S. Whitelam, D. Joester, H. Zhang, J. D. Rimer, A. Navrotsky, J. F. Banfield, A. F. Wallace, F. M. Michel, F. C. Meldrum, H. Cölfen, P. M. Dove, *Science* **2015**, *349*, aaa6760, DOI: 10.1126/science.aaa6760.
[25] R. L. Penn, J. F. Banfield, *Science* **1998**, *281*, 969–971.
[26] F. C. Meunier, D. Verboekend, J. P. Gilson, J. C. Groen, J. Pérez-Ramírez, *Microporous Mesoporous Mater.* **2012**, *148*, 115–121.
[27] M. Choi, K. Na, J. Kim, Y. Sakamoto, O. Terasaki, R. Ryoo, *Nature* **2009**, *461*, 246–249.
[28] X. Zhang, D. Liu, D. Xu, S. Asahina, K. A. Cychosz, K. V. Agrawal, Y. Al Wahedi, A. Bhan, S. Al Hashimi, O. Terasaki, M. Thommes, M. Tsapatsis, *Science* **2012**, *336*, 1684–1687.

Received: August 29, 2016
Revised: October 11, 2016
Published online: October 31, 2016